**Proceedings of the ASME 2016 International Design Engineering Technical Conferences & Computers and Information in Engineering Conference**
**IDETC/CIE 2016**
**August 21-24, 2016, Charlotte, NC, USA**

**DETC2016/CIE-60140**

# MASS CUSTOMIZATION: REUSE OF DIGITAL SLICING FOR ADDITIVE MANUFACTURING

**Tsz-Ho Kwok[1], Hang Ye[2], Yong Chen[1], Chi Zhou[2]*, and Wenyao Xu[3]**

[1]Epstein Department of Industrial and Systems Engineering
University of Southern California, Los Angeles, CA 90089

[2]Department of Industrial and Systems Engineering
[3]Department of Computer Science and Engineering
University at Buffalo, The State University of New York, Buffalo, NY 14260

Email: tszhokwo@usc.edu, hye2@buffalo.edu, yongchen@usc.edu, chizhou@buffalo.edu, wenyaoxu@buffalo.edu

## ABSTRACT

*Additive manufacturing, also known as 3D printing, enables production of complex customized shapes without requiring specialized tooling and fixture, and mass customization can then be realized with larger adoption. The slicing procedure is one of the fundamental tasks for 3D printing, and the slicing resolution has to be very high for fine fabrication, especially in the recent developed Continuous Liquid Interface Production (CLIP) process. The slicing procedure is then becoming the bottleneck in the pre-fabrication process, which could take hours for one model. This becomes even more significant in mass customization, where hundreds or thousands of models have to be fabricated. We observe that the customized products are generally in a same homogeneous class of shape with small variation. Our study finds that the slicing information of one model can be reused for other models in the same homogeneous group under a properly defined parameterization. Experimental results show that the reuse of slicing information have a maximum of 50 times speedup, and its utilization is dropped from more than 90% to less than 50% in the pre-fabrication process.*

**Keywords:** *Mass Customization, Slicing, 3D Printing, Additive Manufacturing, CLIP, Parameterization.*

## 1 Introduction

### 1.1 Background: 3D Printing & Mass Customization

Manufacturing and production has been a big contributor to improved quality and sustainability of human life. Current market trends, such as consumer demand for variety, short product life cycles, high product quality and low cost, have resulted in the need for efficient, responsive, robust and sustainable manufacturing and production paradigm. The traditional mass production of standardized goods has been the source of the nation's economic strength and leadership position in the last century; however, it is also because of mass production that we are losing the competitiveness as it cannot handle the ever changing turbulent market environment. Innovative practitioners begin to throw away the old paradigm of mass production and find their way to a new paradigm, mass customization, by creating variety and customization through flexibility and quick responsibility to meet customers' diverse and ever changing needs at near mass production prices [1]. However, customized product is very challenging to be mass-produced in traditional manners, and the business has to wait for today's advanced technologies to enable profitable customization [2].

As an emerging and advanced technology, additive manufacturing (3D printing) can fabricate parts directly from 3-

*Corresponding author. Phone: (716) 645-4706 Fax: (716) 645-3302

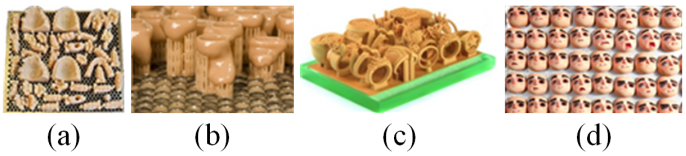


**FIGURE 1**. Mass customization applications of 3D printing in different industrial fields: (a) dental industry [5], (b) medical industrial [6], (c) jewelry industry [7], (d) entertainment industry [8].

Dimensional (3D) digital models without part-specific tooling and fixtures [3]. Thus it provides tremendous flexibility and significantly shortens product development cycle while satisfying customized design requirements without cost penalties. Recent advancements in material, process, and machine development have enabled 3D printing processes to evolve from prototyping usage to end-use product manufacturing [4]. Coupled with advanced 3D scanning and modeling technology, 3D printing technology has the big potential to enable mass customization and push the current marketplace to the new frontier in business competition. Advanced 3D scanning technologies allows for fast and accurate shape retrieving for complex models such as human body, which opens up great opportunities for highly individualized products that are tailored to fit the needs for a specific customer. Innovative companies, especially the ones that provide human centered products and services, are already embracing the new mass customization paradigm by making use of the unique design freedom offered by 3D printing techniques [4]. FIGURE 1 shows the mass customization applications of 3D printing in different industrial fields.

### 1.2 Challenges: Computational Bottleneck

The unique capabilities of 3D printing technologies enable new opportunities for customization, very significant improvement in product performance, multi-functionality and lower overall manufacturing costs. In typical 3D printing systems such as Stereo-Lithography Apparatus (SLA) or Selective Laser Sintering (SLS) machines, hundreds or thousands of customized parts with different shapes can be built at the same time in a single machine. Therefore, mass customization, instead of mass production, can be realized quite readily. However, the lack of computational tools for mass customization, rather than limitations of the hardware, is the key limitation when considering 3D printing for mass customization. The input digital model for 3D printing represents the object boundary by tessellating the surface with finite number of triangles. A complex model requires a large number of triangle facets for sufficient dimensional accuracy and surface smoothness, which will dramatically increase the computational cost of geometrical operations including contour slicing and tool path planning etc.

The customized products share the characteristics of high

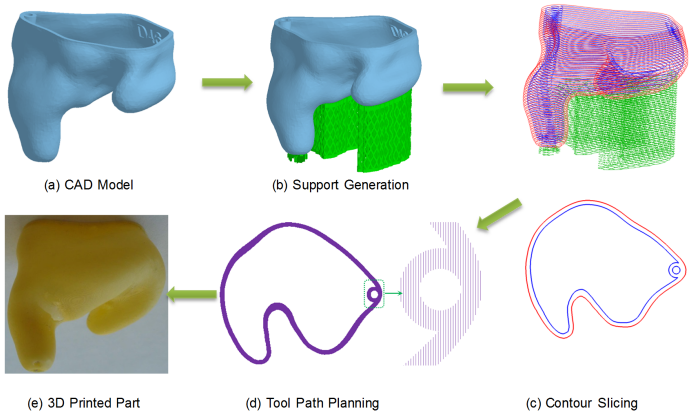


**FIGURE 2**. The state-of-the-art flow of pre-fabrication computation in additive manufacturing.

level of sophistication and complexity. For a decent hearing aid model or human teeth model, more than 100,000 triangles are required to guarantee the geometry fidelity and part accuracy. For a typical SLA machine, the vertical resolution of 25-100$\mu$m reflected by the layer thickness can be easily achieved, consequently thousands of layers and millions of intersection points will be generated for a typical hearing aid model. With the advancement of process and machine development, it is expected higher physical resolution will be used in the near future. Higher resolution will casuse increased number of layers and more complex shape for each layer, and thus larger burden will be imposed on the computational tools. It becomes even more challenging when the computation is taking place in the mass customization environment, where hundreds of complex models have to be processed.

Very recently, Tumbleston et al. [9] proposed a continuous liquid interface production (CLIP) approach to continuously grow objects from a pool of liquid material instead of printing them layer-by-layer. It has proven to be 25-100 times faster (complex products can be printed in minutes instead of hours) than what is available in the market today and has the potential to revolutionize manufacturing. The continuous mode is an indication of infinite thin layer or infinite number of layers which dramatically increased geometry processing burden in pre-fabrication stage. As such, the continuous 3D printing opens the door for mass customization with fully ready hardware support. However, the pre-fabrication computation framework becomes the major bottleneck that hinders the realization of the industrial revolution introduced by 3D printing.

FIGURE 2 shows the standard flow of the 3D printing process which directly converts a digital model in FIGURE 2(a) into a physical object in FIGURE 2(e). Due to the complex features, the digital model of mass customized object requires a large number of triangle facets for sufficient dimensional accuracy and

**FIGURE 3**. Two tooth aligner models share 99% of similarity. The left is for phase 0-30 days, and the right is for phase 31-90 days.

surface smoothness, which will dramatically increase the computational cost of geometric operations for pre-fabrication. For example, in order to fabricate one single hearing aid part with enough comfort in the ear, more than 1 million triangles are required to represent the digital model to guarantee the geometry fidelity and part accuracy. With the CLIP technology, the pre-fabrication time would be in the order of 10 hours, while the actual printing time is in the order of 10 minutes. Therefore, the pre-fabrication has become the bottleneck in 3D printing, and there is an urgent need to devise a new paradigm to accelerate the pre-fabrication of 3D printing in mass customization.

### 1.3 Proposed Solution: Information Reuse

Although 3D model has a very high complexity to process, the mass customized digital models share the characteristics of high similarity. For example, all the hearing aid models possess the same features with slightly variation in terms of size, orientation and shape deformation (more than 97% similarity on average). FIGURE 3 shows an example of two different tooth aligner models which hold the similarity up to 99%. In traditional pre-fabrication process, each digital model will independently go through the aforementioned geometrical operations, and the majority of pre-fabrication computation is redundant and repetitive.

It is this knowledge underneath the shape similarity that potentially provides us the opportunity to redesign the computational paradigm for mass customization in 3D printing. Inspired by this observation, we proposed a brand new computational paradigm to fully take advantage of the high similarity in mass customization. Our argument is that the computational paradigm of 3D printing in mass customization should not repeat the same pre-fabrication computation among different design models. Ideally, the major geometric computation will only be conducted once for the 99% similarity portion, based on which, local modification will be applied to the 1% variation portion. On the basis of this argument, we presented a new computational paradigm of 3D printing for efficient mass customization. This paradigm exploits the similarity of models in mass customization, avoids redundant computation, and only processes the unique region of each model. Therefore, the new paradigm has the potential to gain orders of magnitude improvement in the run time. The detailed approaches will be explained in the following section.

As in the early stage of the exploration on the new paradigm, we are mainly focusing on one of most important pre-fabrication procedures, i.e., contour slicing, in this paper. Note that the proposed strategy is extensible and applicable to all the other pre-fabrication procedures such as tool path planning, support generation etc. Our major contributions are summarized as follows:

1. We developed a novel framework that can significantly reduce the time of pre-fabrication for additive manufacturing.
2. We compute and make use of the bijective mapping between different custom products to enable the reuse of slicing.
3. An efficient mapping optimization is developed to ensure valid images can be generated from the transferred slicing.

Two main test cases commonly used in medical applications: teeth aligner and hearing aid, are used to demonstrate the capability and effectiveness of the proposed framework. Note that both of them are human centered products which require high level of mass customization due to the complex geometry and shape variation, and therefore are well representative of the problem we are addressing in this work. The rest of the paper is organized as follows. The related works are reviewed in the rest of this section. Section 2 gives the overview of the proposed algorithm. The technical details of computing and optimizing the mapping, as well as the slicing reuse is given in Section 3 . The experimental results and physical test cases are shown in Section 4, and the paper is concluded in Section 5.

### 1.4 Related Works

Historically, there are two waves of mass customization: configured mass customization and personalized customization. In configured mass customization, the customers are provided certain number of choices based on a base configuration to achieve variety and individualization. The mode of modification on the base or template inspired us to design different clusters for the models with high similarity in same category, then fine tune the cluster prototype based on the customized information. The cluster based methodology has not been used or explored in literature before. Hildebrand [10] presented a close but not similar idea based on a sketch pipeline for mass customization guiding the process of additive manufacturing. The process starts from sketch-based retrieval of a user sketch in a large 3D model database, then customizes the design by interactive local modification and eventually manufactures the customized 3D shapes using a 3D printer. However, this research work did not contribute on the pre-fabrication computation for 3D printing. Luo [11] proposed a shape-based interpolation technique using distance transform and morphing for three dimensional reconstructions, which is a reverse problem of slicing in 3D printing.

Slicing is one of the most important pre-fabrication procedures in 3D printing. Various methods and algorithms have

been developed to slice the STL files and generate the contours. Two strategies are commonly used for slicing: (1) for each triangle, search for all the slicing planes that pass through it; (2) for each slicing plan, search for all the triangles that have intersections with it. The first strategy can easily identify the intersecting triangles by checking the minimum and maximum $z$ coordinate [12–18]. However, as the intersection points are located at different slicing planes, only disjoint line segments are generated, further steps are needed to form the line segments into loops. The second strategy is commonly used for topology construction based slicing algorithm [19–21]. By travelling along the neighboring triangles, contours on the same slicing plan can be easily constructed. However, locating the starting triangle for the marching process requires substantial computational time. Both of these two strategies are designed for single model slicing rather than mass customization.

Computing the mapping between different models is an essential step to enable the reuse of slicing, and some mapping technologies are reviewed here. When the models are simple, a spherical domain [22] is commonly used, but it fails when the topology of input surfaces is not trivial. Therefore, a more flexible framework is to use complexes based domains [23–26], where surfaces are first segmented into simplicial complexes. The global mapping of an entire model can be obtained by parameterizing the partitions of a mesh surface into its corresponding base domains with the same boundary condition. Praun et al. [23] used the defined connectivity of base domains on a template model as input to construct the domains on different models consistently. Kraevoy et al. [25] and Schreiner et al. [24] further generalized the approach to generate the base domains automatically based on a greedy triangulation method. Kwok et al. [27, 28] developed a domain construction method using Voronoi diagram and a domain optimization method to reduce the mapping distortion. Our study finds that the optimized mapping is a good starting point and foundation for our application.

## 2 Algorithm Overview

Projection based stereo-lithography 3D printing is getting more popular recently. The mask image is one of the most important parameters in projection based stereo-lithography. In order to perform the layered operation, the CAD model is sliced layer by layer. Each layer can be converted into an image (see the top row of FIGURE 4). The layers are defined as the intersection of horizontal 2D planes with the 3D object (STL file). As the plane moves up, successive layers are defined. Each surface that intersects the plane forms a direct line segment on the planar slice. All these intersection lines together will define the contour. However, this process is computationally expensive especially when the mesh size and the number of layers are huge to provide sufficient quality and frames for the CLIP process. This inefficiency becomes the major bottleneck for mass customization, where hundreds or thousands of customized products have to be fabricated.

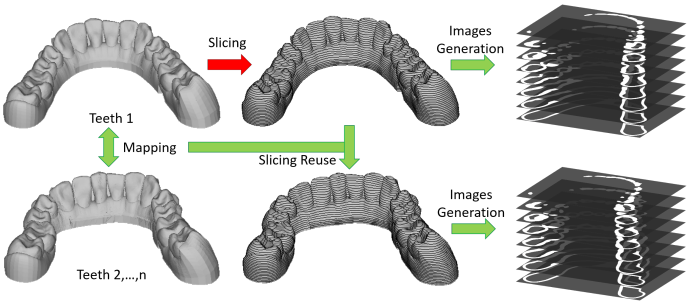


**FIGURE 4**. The overview of the reuse of slicing. (Top row) The traditional pre-fabrication pipeline first slices the input model and then generates the images from the slices. The bottleneck is the slicing process (shown in red arrow). (Bottom row) The proposed pipeline for slicing reuse by computing the mapping between the input models and transfer the slices from the slicing results, bypassing the slicing process.

Our algorithm is based on an observation of the mass customization that a series of customized products is very similar in shape and topology with just a little variation in geometry to fit different individual needs. The basic idea is to modify an existing pre-fabrication information for one of the product in a series, and reuse it for all other products in the same series, in such a way that the complete pipeline of the pre-fabrication process only needs to be done once. FIGURE. 4 shows the concept of the slicing reuse. Assume one of the teeth aligner (Teeth 1) is picked to undergo the standard slicing process, then it is sliced to a set of contours and then mask images are generated for each of the contours. Due to the reason that the slicing process (red arrow) is the bottleneck, our main goal is to bypass this process for other models in the series (Teeth $2 \ldots n$) by making use of the shape similarity between them.

Specifically, a bijective mapping is defined among the series of models $\Gamma^n : M_1 \Rightarrow M_n$, which could be given by the design process [29] or established by cross-parameterization [27, 28]. Because our focus is on the mask images projection where the slices are 2D planes, we further constrain the mapping to be an in-plane mapping by optimizing the positions of vertices in the base domains to align with the isovalues of height. As in the slicing process for model 1, every slice is a contour which is a set of ordered points, and the positions of points are stored in a text file. The points are located exactly on the surface of the model. With the defined mapping $\Gamma$, every point on the model 1 ($p_i \in M_1$) can be found a correspondence in another models ($p_i^n \in M_n$), i.e., $\Gamma^n(p_i) = p_i^n$. Therefore, the slicing can be reused by mapping all the points of contours from model 1 to model $n$, and save it back to a text file with the same ordering and format. As a result, the slicing data is ready for model $n$, and its corresponding mask images can be generated.

If the mapping is not given, it can be computed within few seconds [27], and the computation complexity for mapping all the contour points is linear with each step as quick as a lookup table. This new pre-fabrication pipeline of reusing the slicing data by making use of the model mapping can bypass the long slicing procedure, and it can make 30-50 times speedup for one model. This efficiency is critical when there are many models in a series, and we will demonstrate the occupation of slicing process can be reduced from more than 90% to less than 50% in the total time for the pre-fabrication process. That is, the slicing process is just as fast as the image generation process.

In the following sections, we will give the technical details of the mapping computation and optimization, and the reuse of slicing.


**FIGURE 5**. The capability of cross-parameterization is demonstrated by linear interpolating the positions of vertices between two input hand models at $t = 0$ and $t = 1$.

## 3 Model Mapping and Slicing Reuse

The automatic generation of a 3D model like a human body, face or bone, is very common in the areas of CAD/Computer Graphics and Biomedical Engineering. There is a plethora of applications involved in this process, for example crowd simulation, medical image analysis and customized medical design. This process is crucial because it reduces the reconstruction time of a model, which is vital for fast medical preparation and mass customization. Parametric design [29] and template fitting [30] are the important techniques for mesh reconstruction, especially for the applications which employ bioengineering analysis with the use of Finite Element Method (FEM). This is because the models generated by these method are not only customized and accurate, but also the mesh topology and connectivity are consistent. In other words, the generated models have the bijective mapping among all of them. For the example of teeth aligner shown in FIGURE 4, it is designed by parametric modeling and direct manipulation. Both of the processes maintain the consistency of the mesh, so the mapping is defined among different teeth models. Note that, as the models differ mainly in the $XY$-plane, the mapping itself is nearly an in-plane mapping with just a little variations. Although most of the cases that the series of customized products contain the mapping, we briefly introduce how the mapping is established by using cross-parameterization when it is not given.

### 3.1 Cross-Parameterization

Without loss of generality, assume a bijective mapping is needed for a source model $M_s$ and a target model $M_t$ with different mesh connectivity, vertex number, and face number. The idea is to partition both models in a consistent way to get two abstract layouts of simplicial complex. The two patch layouts $P_s$ and $P_t$ have the same connectivity and are consistent to each other. For each patch $P^i$ in a patch layout, a corresponding planar domain $B^i$ can be designed [31] (e.g., triangular, quadrilateral, circular shapes), and a 3D-to-2D mapping can be obtained.

$$\Gamma_s : P_s^i \Rightarrow B_s^i \quad \text{and} \quad \Gamma_t : P_t^i \Rightarrow B_t^i.$$

The mapping between the base domains, i.e., the 2D-to-2D mapping, can be established as $\Gamma_{st} : B_s^i \Rightarrow B_t^i$ by using barycentric coordinates [32]. Then, the cross-parameterization is established by the two 3D-to-2D and the 2D-to-2D mappings:

$$\Gamma = \Gamma_s \cdot \Gamma_{st} \cdot \Gamma_t^{-1}, \tag{1}$$

where $\Gamma : M_s \Rightarrow M_t$. For more details, readers are referred to [28]. This process is efficient and can be completed within seconds [27]. To demonstrate the capability of the cross-parameterization, we have established the mapping between two hand models with different mesh and shapes shown in FIGURE 5. By aligning the models on a time domain ($t$), where hand models 1 and 2 are put at $t = 0$ and $t = 1$, i.e., $\Gamma(t = 0) = M_s$ and $\Gamma(t = 1) = M_t$, the intermediate ones can be generated by simple linear interpolation of the vertex positions between them. It can be seen that the correspondences between vertices are well-defined and the mapping quality is very good.

### 3.2 Mapping Optimization

The mapping given by the mesh generation methods or computed by cross-parameterization provides the correspondence between different models. This correspondence is actually a general 3D mapping, and can support arbitrary shape difference and deformation. We want it to be an in-plane mapping because we are focusing on generating images that are in 2D plane. Therefore, a mapping optimization for planar constraint is presented here. The objective of the optimization is to incorporate the printing direction in the mapping, and to constrain the mapping varies only in the orthogonal plane of the printing direction. As a result, the mapping in a particular height will be an in-plane mapping.

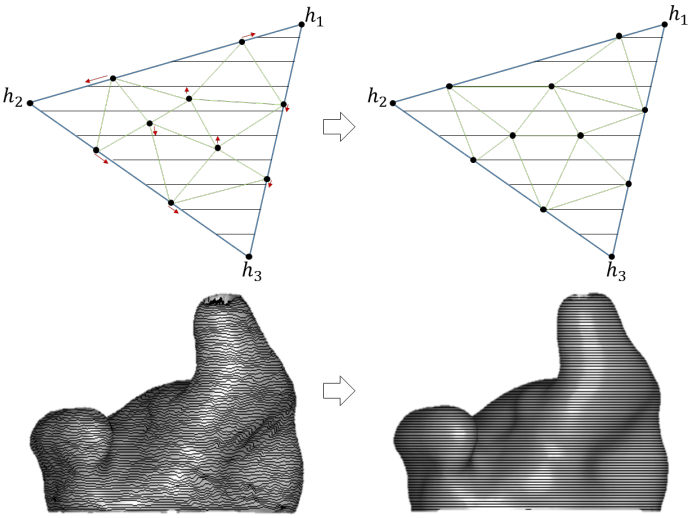


**FIGURE 6**. The mapping optimization constraining the mapping by fixing the height (i.e., $z$ coordinate). The transferred slices are in-plane by the constrained mapping.

Refer to Eq. (1), the cross-parameterization ($\Gamma$) is constituted by three parts : $\Gamma_s$, $\Gamma_{st}$, and $\Gamma_t$. As the base domains ($B_s$, $B_t$) are consistent to each other, the 2D-to-2D mapping $\Gamma_{st}$ for every points in the domain is simply the linear interpolation of the corners of the domains. That is, without loss of generality, for triangular domains, the length ratio and the area coordinate determine the bijective mapping for the boundaries and the interior of the domains respectively. Therefore, the planar constraint can be easily incorporated by modifying the 3D-to-2D mappings ($\Gamma_s$, $\Gamma_t$) to match with the isovalues of height in the base domains. As long as both of the mappings can successfully achieve the same goal for the value of height, then the points in $M_s$ will be mapped to the points in $M_t$ with the same height, because $\Gamma_{st}$ is a linear mapping. Noted that, the two 3D-to-2D mappings are independent to each other, and therefore, this optimization is linear and can be solved efficiently.

Specifically, assume a triangular domain having three corner points ($\mathbf{p}_1, \mathbf{p}_2, \mathbf{p}_3$), with the 3D coordinates $\mathbf{p}_i : [x_i, y_i, z_i]$. For the building direction in $z$ axis, then the height for the corner points are their $z$ coordinates, i.e., $h_1 = z_1$, $h_2 = z_2$, and $h_3 = z_3$. The points construct a plane, and they are converted to a 2D coordinate system in $(u, v)$. By applying a proper rotational matrix, the $z$ axis in 3D can be aligned with the $v$ axis in the 2D coordinate system as shown in the top row of FIGURE 6. Therefore, the $v$ axis is exactly the representation of height, and a set of isovalues of height can be easily drawn by a set of horizontal lines. The basic idea of the optimization is to project every vertex in 2D mapped by the 3D-to-2D mappings ($\Gamma_s$ or $\Gamma_t$) to align with the isoline of height that it belongs to. The implementation of this is actually straightforward. The computation of the 3D-to-2D mapping can be based on the mean value coordinate [33] of each vertex and its neighboring vertices. Similar to Finite Element Method, every vertex has a set of equations related to its neighbors, and the union of all the equations make a linear equation system with the variables are the vertex positions in 2D $(u, v)$. Constraining the mapping being in-plane is setting the $v$ coordinates as the height values and removing them from the variables. As a result, the solution of the equation system will just optimize the $u$ coordinates with the $v$ coordinates well-aligned with the isovalues of height, and the mapping is optimized. The bottom row of FIGURE 6 shows the transferred slices before and after the optimization. Remarked that, the optimization does not create any additional burden to the computation, instead it speeds up the process because the size of the linear equation system is reduced by half.

### 3.3 Slicing Reuse

Given a STL file, which is the input CAD model and it is represented by a number of faces stored by their vertices, the traditional slicing process is to intersect the model with a set of horizontal planes and result in a set of intersection points on the faces. The points can be reordered based on the neighborhood relationship between the faces, and the collections of the ordered points are the contours. There could be multiple contours at a particular height, but they are all exported in one file, where each contour is stored as a series of points in the format of $(x_1\ y_1\ z_1\ x_2\ y_2\ z_2\ \cdots)$. Besides this contour file, to enable the reuse of slicing, another file recording the relationship between the contours and the CAD model is also exported. The contours and the CAD model are related by where the points of the contour are located on the model. Specifically, as a contour point is the intersection point on the CAD model, it must lie on the model in a particular face. Therefore, by recording which face ($f$) a point belongs to and the area coordinate ($\lambda_1\ \lambda_2\ \lambda_3$), the point ($\mathbf{p}$) can be expressed by the vertices of the face as

$$\mathbf{p} = \lambda_1 f.\mathbf{v}_1 + \lambda_2 f.\mathbf{v}_2 + \lambda_3 f.\mathbf{v}_3, \tag{2}$$

where $\lambda_1, \lambda_2, \lambda_3 \geq 0$ and $\lambda_1 + \lambda_2 + \lambda_3 = 1$. We call this file the encoding file, because every intersection point is encoded by a face ID and area coordinate.

Contour files can be generated by a STL file and the encoding files. Reading the encoding file, the face IDs are used to locate the corresponding faces in the CAD model, and together with the area coordinates, all the positions of points can be computed by Eq. (2). Assume the vertex positions of the CAD model are changed, a different set of contour files will be generated by the same encoding file. For a series of models with the mapping defined among them, the mapping $\Gamma$ is able to find for every vertex of one model the corresponding positions in other modes. As a result, the vertex positions of the CAD model can be changed

**TABLE 1**. Table of time statistics

| Model | Size | #L | $T_{slice}$ | $T_{S2I}$ | $T_{reuse}$ |
|---|---|---|---|---|---|
| Teeth Aligner | 545k | 14k | 2h8m | 5m21s | 2m42s |
| Hearing Aid | 327k | 8.8k | 10m29s | 1m | 17s |

The time units are in hour (h), minute (m) and second (s). The size of model is reported as the number of faces. #L is the number of layers. $T_{slice}$, $T_{S2I}$ and $T_{reuse}$ are the times for slicing, image generation from slices and slicing reuse.

for other models in the series, and the contours can be customized individually with the same encoding file.

## 4 Results

We have applied our developed framework to two common cases in medical applications: teeth aligner and hearing aid. The two cases also have a great demand of mass customization, both in different stages of the same client or among different clients. The experimental tests are run on a PC with Intel(R) Core(TM) i7-4790 CPU @3.60GHz, 8GB RAM, and the layer thickness is set to $1\mu m$ for a sufficient resolution for the CLIP process. The time statistics of the two test cases are summarized in Table 1.

The teeth model has a model size of 273k vertices and 545k faces. It is oriented as shown in FIGURE 7 with the $z$ axis (building direction) pointing out of the paper. The height of the model is $14.484mm$, and thus there are 14484 layers in total. In the traditional way, slicing on teeth model takes 2 hours and 8 minutes, where generating images from the slices takes 5 minutes and 21 seconds, so the total time for each teeth model will be 2 hours and 13 minutes. It can be seen that the slicing procedure is the major bottleneck of the pre-fabrication process. Assume there are 100 models to be fabricated, the total time for the slicing and generating images will be more than 9 days, where the slicing time occupies 96% of the total time. It is ironic that the CLIP process speeds up the fabrication time from hours to minutes, but the pre-fabrication time is increased from minutes to hours. Fortunately, if the slicing information can be transferred and reused by the mapping defined between models, then no slicing is needed for other models. The reuse of slicing takes only 2 minutes and 42 seconds for one model, so the total time for each transferred model will be (2 minutes and 42 seconds) + (5 minutes and 21 seconds) = 8 minute and 3 seconds. For 100 models, the total time will be (2 hours and 13 minutes) + 99 $\times$ (8 minutes and 3 seconds) = 15.5 hours, in which the slicing and transferring time occupies only 43% of the total time. FIGURE 7 shows the mask images that are generated for the traditional slicing for Teeth 1 and the reused slicing for Teeth 2, as well as the fabricated parts, respectively. To validate the proposed method in terms of accuracy, we have applied the traditional slicing for Teeth 2 and compared its mask images to those of the reused slicing. The mask images are the binary images with only 0 or 1 in each pixel, and the similarity of two mask images are measured by counting the number of corresponding pixels in the images are the same, i.e.,

$$S(I_1, I_2) = \frac{\sum_i^w \sum_j^h [I_1(i,j) = I_2(i,j)]}{w \times h},$$

where $w$ and $h$ are the width and height of the images $(I_1, I_2)$. We have compared all the pairs of the mask images in the same layer from the direct slicing and the reused slicing. All the pairs have the similarity greater than 99.99%, and the least similar one has only 4 pixels different (image size is $1024 \times 768$). The statistics has shown that adopting the proposed work can greatly reduce the computational time without the loss of geometric accuracy.

Another test case is the hearing aid, which is a smaller model with the size of 164k vertices and 327k faces. Similarly, it is oriented as shown in FIGURE 8 with the $z$ axis (building direction) pointing out of the paper. The height of the model is $8.789mm$, and there are 8789 layers. Slicing the hearing aid model takes 10 minutes and 29 seconds, where generating images from the slices takes 1 minute. Again if there are 100 models to be fabricated, the total time for the slicing and generating images will be more than 19 hours, where the slicing time occupies 91% of the total time. With the defined mapping, the reuse of slicing takes 17 seconds, and the total time will be (11 minutes and 29 seconds) + 99 $\times$ (1 minutes and 17 seconds) = 138 minutes 32 seconds, in which the slicing and transferring time occupies only 28% of the total time. The mask images for both cases and the corresponding fabricated parts are shown in FIGURE 8.

In order to verify the effectiveness, physical parts are also printed on a homemade machine based on CLIP technology. The mask images generated from the proposed new pre-fabrication pipeline are utilized as the frame of the video projection to grow the batch of mass customized parts. FIGURE 9(a) and (b) show the digital models and FIGURE 9(c) and (d) show the printed parts. The fabrication time is around 10 minutes for the hearing aid and 4 minutes for teeth aligner, which are well comparative to the computational time of pre-fabrication using the proposed method.

## 5 Discussion and Conclusion

In this paper, we have presented a new pre-fabrication pipeline to reuse slicing information for additive manufacturing especially for the Continuous Liquid Interface Production (CLIP) process. Our observation is that although there are many customized products have to be fabricated in mass customization, they are similar in shape, and a bijective mapping between them are defined or can be easily established. Taking advantages of the mapping, the sliced contours can be transferred and reused, and thus only one time of slicing has to be preformed. We have

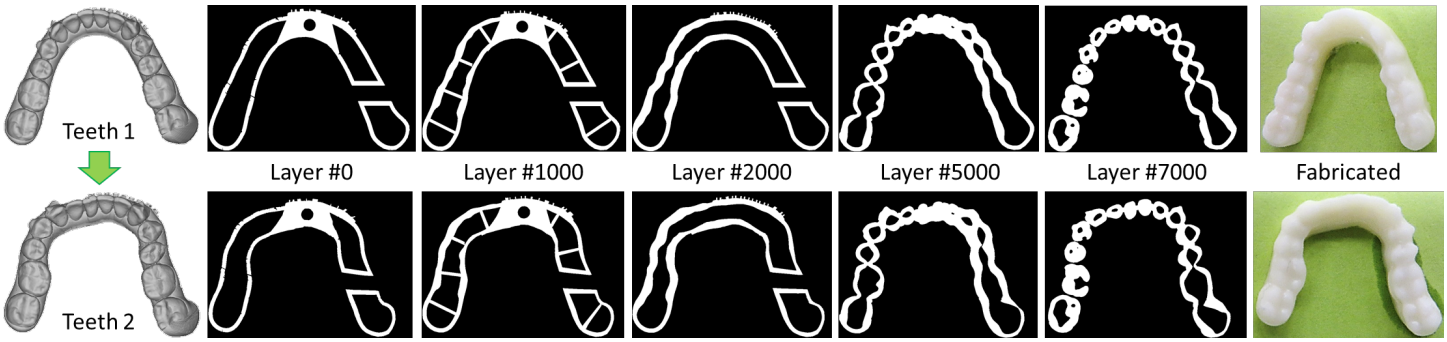


**FIGURE 7**. The mask images in the top row are generated from the contours that are directly slicing on the model of Teeth 1. Those in the bottom row are generated from the reused slices that are computed based on the mapping from Teeth 1 to 2. The fabricated parts are shown in the right.

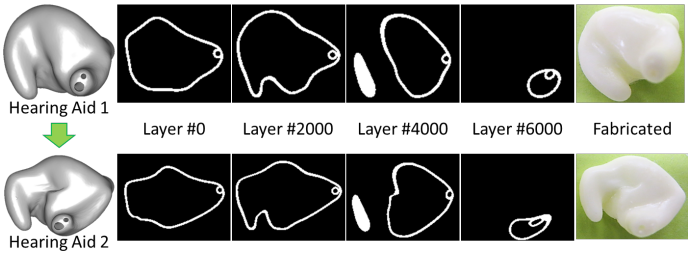


**FIGURE 8**. The mask images in the top row are generated from the contours that are directly slicing on the model of Hearing Aid 1. Those in the bottom row are generated from the reused slices. The fabricated parts are shown in the right.

presented the techniques for establishing an in-plane mapping among different models as well as the reuse of slicing. Valid mask images can be directly generated from the reused slicing. Noticed that, although we focus on the mask-image-projection-based fabrication method, the slices of which are planes, it is not necessary to be planar. This framework is general for all kind of slice/planning including non-planar ones (e.g., CNC tool path). For non-planar reusing, optimization to in-plane is not needed, and it will be our future work to study the performance of the framework in the non-planar cases. The experimental tests have demonstrated the effectiveness and the efficiency of the framework. The pre-fabrication process can be speeded up to more than 30 times, and the occupation of slicing in the throughput can be reduced from nearly 90% to less than 50%.

One of the limitations in this framework is that it can only work on the models with shape difference mainly in the horizontal plane, i.e., perpendicular to the building direction. For the models having shape difference in the building direction, the topology of each slice is changed, and the current framework is not able to handle that. Our future will extend our framework to handle this kind of topology changes. A possible solution is making use of the defined mapping to trace the vertical difference, and contours will be added or removed in an adaptive way.

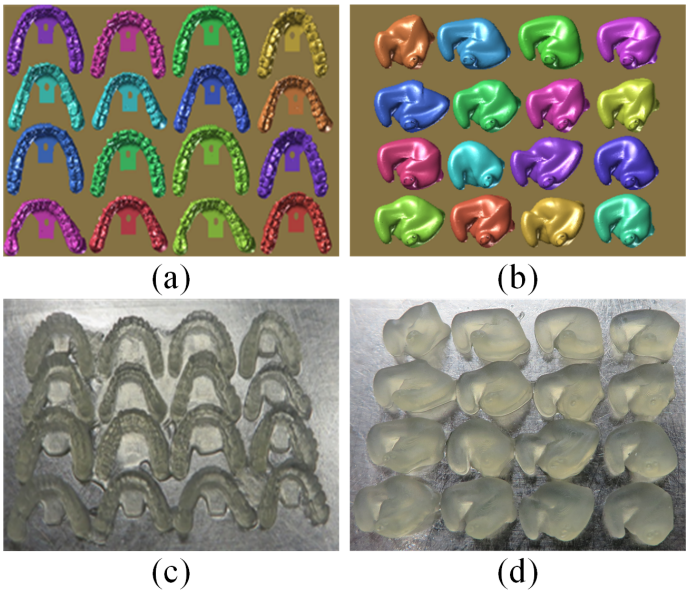


**FIGURE 9**. Physical test cases: (a) digital models of aligners and (b) hearing aids; (c) printed aligners and (d) hearing aids.

## ACKNOWLEDGMENT

The authors are grateful for financial support from National Science Foundation (NSF) through CNS-1547167.

## REFERENCES

[1] Pine, B. J., 1993. *Mass customization: The new frontier in business competition*. Harvard Business School Press, Boston, MA.

[2] Bourell, D. L., Leu, M. C., and Rosen, D. W., 2009. Roadmap for Additive Manufacturing: Identifying the Future of Freeform Processing. Tech. rep., The University of Texas at Austin, Austin, TX.

[3] Gibson, I., Rosen, D. W., and Stucker, B., 2009. *Additive*

*Manufacturing Technologies: Rapid Prototyping to Direct Digital Manufacturing*, 1st ed. Springer.

[4] Wohlers, T., 2013. Wohlers Report: Additive Manufacturing and 3D Printing State of the Industry. Tech. rep., Wohlers Associates, Fort Collins, CO.

[5] Huang, X., Leng, T., Zhu, M., Zhang, X., Chen, J., Chang, K., Aqeeli, M., Geim, A. K., Novoselov, K. S., and Hu, Z., 2015. "Highly flexible and conductive printed graphene for wireless wearable communications applications". *Scientific Reports,* ***5***(18298(2015)), pp. 1–8.

[6] Calvert, P., 2001. "Inkjet printing for materials and devices". *Chemistry of materials,* ***13***(10), pp. 3299–3305.

[7] Singh, M., Haverinen, H. M., Dhagat, P., and Jabbour, G. E., 2010. "Inkjet printing-process and its applications". *Advanced materials (Deerfield Beach, Fla.),* ***22***(6), pp. 673–685.

[8] Hebner, T. R., Wu, C. C., Marcy, D., Lu, M. H., and Sturm, J. C., 1998. "Ink-jet printing of doped polymers for organic light emitting devices". *Applied Physics Letters,* ***72***(5), pp. 519–521.

[9] Tumbleston et al., 2015. "Continuous liquid interface production of 3D objects". *Science,* ***347***(6228), pp. 1349–1352.

[10] Hildebrand, K., and Alexa, M., 2013. "Sketch-based pipeline for mass customization". In Proceedings of ACM SIGGRAPH 2013 Talks, ACM, p. 1.

[11] Luo, B., and Hancok, E. R., 1997. "Slice interpolation using the distance transform and morphing". In Proceedings of 13th International Conference on Digital Signal Processing, Vol. 2, pp. 1083–1086.

[12] Kirschman, C. F., and Jara-Almonte, C. C., 1992. "A parallel slicing algorithm for solid freeform fabrication processes". In Proceedings of International Solid Freeform Fabrication Symposium, pp. 26–33.

[13] Cao, W., and Miyamoto, Y., 2003. "Direct slicing from AutoCAD solid models for rapid prototyping". *INT J ADV MANUF TECH,* ***21***(10), pp. 739–742.

[14] Chakraborty, D., and Choudhury, A. R., 2007. "A semi-analytic approach for direct slicing of free form surfaces for layered manufacturing". *Rapid Prototyping Journal,* ***13***(4), pp. 256–264.

[15] Starly, B., Lau, A., Sun, W., Lau, W., and Bradbury, T., 2005. "Direct slicing of STEP based NURBS models for layered manufacturing". *Computer-Aided Design,* ***37***(4), pp. 387–397.

[16] Sun, S., Chiang, H., and Lee, M., 2007. "Adaptive direct slicing of a commercial CAD model for use in rapid prototyping". *INT J ADV MANUF TECH,* ***34***(7), pp. 689–701.

[17] Tata, K., Fadel, G., Bagchi, A., and Aziz, N., 1998. "Efficient slicing for layered manufacturing". *Rapid Prototyping Journal,* ***4***(4), pp. 151–167.

[18] Liao, Y.-S., and Chiu, Y.-Y., 2001. "A new slicing procedure for rapid prototyping systems". *The International Journal of Advanced Manufacturing Technology,* ***18***(8), pp. 579–585.

[19] Rock, S. J., and Wozny, M. J., 1991. "Utilizing topological information to increase scan vector generation efficiency". In Proceedings of International Solid Freeform Fabrication Symposium, pp. 28–36.

[20] Rock, S. J., and Wozny, M. J., 1992. "Generating topological information from a "bucket of facet"". In Proceedings of International Solid Freeform Fabrication Symposium, pp. 251–259.

[21] Mcmains, S., and Séquin, C., 1999. "A coherent sweep plane slicer for layered manufacturing". In Proceedings of the 5th ACM Symposium on Solid Modeling and Applications, pp. 285–295.

[22] Praun, E., and Hoppe, H., 2003. "Spherical parametrization and remeshing". In SIGGRAPH, ACM, pp. 340–349.

[23] Praun, E., Sweldens, W., and Schröder, P., 2001. "Consistent mesh parameterizations". In SIGGRAPH, ACM, pp. 179–184.

[24] Schreiner, J., Asirvatham, A., Praun, E., and Hoppe, H., 2004. "Inter-surface mapping". *ACM Trans. Graph.,* ***23***(3), pp. 870–877.

[25] Kraevoy, V., and Sheffer, A., 2004. "Cross-parameterization and compatible remeshing of 3d models". *ACM Trans. Graph.,* ***23***(3), pp. 861–869.

[26] Pietroni, N., Tarini, M., and Cignoni, P., 2010. "Almost isometric mesh parameterization through abstract domains". *IEEE Trans. Vis. and Comp. Graph.,* ***16***(4), pp. 621–635.

[27] Kwok, T.-H., Zhang, Y., and Wang, C. C. L., 2012. "Constructing common base domain by cues from voronoi diagram". *Graphical Models,* ***74***(4), pp. 152 – 163.

[28] Kwok, T.-H., Zhang, Y., and Wang, C. C. L., 2012. "Efficient optimization of common base domains for cross parameterization". *IEEE Transactions on Visualization and Computer Graphics,* ***18***(10), Oct, pp. 1678–1692.

[29] Chu, C.-H., Tsai, Y.-T., Wang, C. C. L., and Kwok, T.-H., 2010. "Exemplar-based statistical model for semantic parametric design of human body". *Computers in Industry,* ***61***(6), pp. 541 – 549.

[30] Kwok, T.-H., Yeung, K.-Y., and Wang, C. C. L., 2014. "Volumetric template fitting for human body reconstruction from incomplete data". *Journal of Manufacturing Systems,* ***33***(4), pp. 678 – 689.

[31] Floater, M., 1997. "Parametrization and smooth approximation of surface triangulations". *Comput. Aided Geom. Des.,* ***14***(3), pp. 231–250.

[32] Floater, M., 2003. "Mean value coordinates". *Comput. Aided Geom. Des.,* ***20***(1), pp. 19–27.

[33] Ju, T., Schaefer, S., and Warren, J., 2005. "Mean value coordinates for closed triangular meshes". *ACM Trans. Graph.,* ***24***(3), July, pp. 561–566.